

# New Methodologies for Grain Boundary Detection in EBSD Data of Microstructures

Rick Catania\* and Arulmurugan Senthilnathan<sup>†</sup> *Virginia Tech, Blacksburg, 24061, VA, USA* 

John Sions<sup>‡</sup>, Kyle Snyder<sup>§</sup>, Huda Al-Ghaib<sup>¶</sup>, and Ben Zimmerman<sup>∥</sup> Commonwealth Center for Advanced Manufacturing, Prince George County, VA 23842

Pınar Acar\*\*
Virginia Tech, Blacksburg, 24061, VA, USA

This work discusses new methodologies for identifying the grain boundaries in color images of metallic microstructures and the quantification of their grain topology. Grain boundaries have a large impact on the macro-scale material properties. Particularly, this work employs the experimental microstructure data of Titanium-Aluminum alloys, which can be used for various aerospace components owing to their outstanding mechanical performance in elevated temperatures. The grain topology of these metallic microstructures is quantified using the concept of shape moment invariants. In order to capture the grains using the shape moment invariants, it is necessary to identify the grain boundaries and separate them from their respective grains. We present two methodologies to detect the grain boundaries. The first method is the tolerancebased neighbor analysis. The second method focuses on creating three-dimensional space of pixel intensity values based on the three color channels and measuring the Euclidean distance to separate different grains. Additionally, since the grain boundaries may not possess the same material properties as the grain itself, this work investigates the effect of including the grain boundaries when determining the homogenized material properties of the given microstructure. To generate adequate statistical information, microstructures are reconstructed from the experimental data using the Markov Random Field (MRF) method. Upon separating the grains, we use the shape moment invariants to quantify the shapes of different grains. Using the shape moment invariants and the experimental material property values, three neural network functions are developed to investigate the effects of grain boundaries on material property predictions.

#### **Nomenclature**

 $\eta$  = Normalized central moment

 $\omega$  = Dimensionless shape moment invariant

 $\phi$  = Hu moment

 $\theta$  = Direction of intensity gradient

 $A_g$  = Grain area  $A_t$  = Total area

G = Magnitude of intensity gradientODF = Orientation distribution function

VF = Volume fraction

<sup>\*</sup>Graduate Research Assistant, M.Sc. Student, AIAA Student Member

<sup>&</sup>lt;sup>†</sup>Graduate Research Assistant, Ph.D. Student, AIAA Student Member

<sup>‡</sup>Materials Research Engineer

<sup>§</sup>Materials Research Engineer

<sup>¶</sup>Senior Research Engineer

R&D Manager

<sup>\*\*</sup> Assistant Professor, AIAA Member

#### I. Introduction

Titanium-Aluminum alloys are commonly used in aerospace systems because they provide improvements in weight and mechanical strength. The material properties and performance of a large-scale component rely on the features of the underlying microstructures, including grain shape, orientation, and the presence of grain boundaries between distinct grains. The microstructural orientations are typically visualized using Electron Backscatter Diffraction (EBSD) [1–6]. In an EBSD sample, different grain orientations are represented by their pixel intensity values in the three RGB (Red-Green-Blue) color channels. Due to the time and financial expense of producing samples, it is beneficial to develop a method that enables the investigation of the material features in larger domains.

Grain boundary detection has been attempted in the past mostly for the gray-scale images and for the color microstructural images, while the previous methodologies were not very accurate in edge detection [7, 8]. In this study, we focus on detecting the grain boundaries of color microstructure images using tolerance-based neighbor analysis and Euclidean-distance methodologies. The main goal is to detect the grain boundaries in the microstructure sample, quantify the grain texture, and ultimately develop a reconstruction methodology using machine learning technique with the integration of shape moment invariants in future work. In order for the shape moment invariants to be identified, an image processing technique must be applied to separate the grains of microstructure. This work explores two image processing techniques that will separate the grains by identifying the grain boundaries in EBSD images. From this, neural networks will be trained using Bayesian regularization to predict material properties from the shape moment invariant values.

The first proposed method is the neighbor analysis technique which in general means including the neighborhood information to classify data. Various forms of this method have been explored in the past for diverse applications [9, 10]. Here, the goal of this method is to identify the grain boundary in an EBSD image using the available neighborhood information for a given pixel. This goal is achieved by establishing a tolerance value for the RGB intensity values of the pixels when compared to the neighbor. When the difference value for the RGB color channels between neighboring pixels is below the tolerance value, they are considered being of the same grain. Inversely, when the difference value is above the tolerance value, a boundary is created. When this technique is applied to images of EBSD data, it is possible to outline each of the grains as well as index the number of grain shapes present in the sample. The homogenized material properties of the microstructure are determined by averaging the material properties of the specific grains based on their respective presence in the microstructure. Including the grain boundaries is necessary because they account for a significant amount of pixels in a microstructure sample. With this method, the presence of these grain boundaries can be factored into the overall microstructure. The other grain boundary detection explored in this work is similar to the first method in terms of the neighbor analysis, but the comparisons are made by evaluating the pixel intensity values in 3-D cartesian coordinate space rather than using a tolerance range. When the intensity values are represented in 3-D cartesian coordinate space, it is possible to measure the Euclidean distance between RGB intensity values of different pixels. The Euclidean distance method is a common method that has been explored in the past for detecting grain boundaries [11]. Previous work calculated Euclidean distance based on a criterion of similarity using a given data point and region, but this work calculates Euclidean distance with respect to the list of nearest neighbors for a given pixel in an image. Both methods have the additional benefit of storing the percentage of boundary pixels in the microstructure. The grain boundary has different material properties than either of its corresponding grains, meaning it will be important to consider their effect on the overall microstructure.

These two methods are also be compared to the Canny Edge Detection method in the Python library [12], a standard edge detection technique. This technique is a multi-stage process which involves noise reduction using a 5x5 Gaussian filter, intensity gradient identification, non-maximum suppression, and hysteresis thresholding [12], which will be discussed more in the subsequent sections of this work. This method proves to be an effective method to identify the edges present in image data. It is often applied to areas such as facial recognition and obstacle identification for autonomous vehicles [12]. However, the main drawback is that it functions by converting RGB image data to gray-scale, thus neglecting the necessary information to identify different grains using the color intensity values. Therefore, the present work will investigate the effectiveness of both of the image processing techniques to characterize the grain boundaries of metallic microstructures.

The paper is structured as follows. Section II explores the mathematical formulation that is used to quantify the microstructural grain shapes. Section III explains the two grain boundary identification techniques mentioned above. This is followed by the discussion of the application of shape moment invariants to the processed image data in order to train a neural network capable of predicting material property values in Section IV. The work summary and future plans of this research are found in Section V.

## II. Comparison of Tolerance-based Neighbor Analysis and Euclidean Distance to Canny Edge Detection

In order to apply shape moment invariants to the EBSD data at the local level for a given microstructure, it is necessary to detect distinct grains that are differentiable from their neighboring grains. To do this, two methods are investigated. The first method is developed by the authors and it uses a tolerance-based neighbor analysis between the pixel intensity values for the RGB color channels. Each pixel has an intensity value for each of the three color channels ranging from 0 to 255. These values are then converted to the decimal scale by normalizing with respect to 255 and stored for each pixel location. The proposed method compares the color intensity values of a given pixel on a scale of 0 to 1 to each of its immediate neighbors using an acceptable tolerance value that indicates whether the pixel is of the same grain as its neighbors. Based on a trial-and-error method, the tolerance value is defined as a 25 percent difference between each of the RGB intensity values for the pixel in question and those of its corresponding neighbors. When a pixel is outside the tolerance range, it is considered to be a part of the grain boundary and is labeled as such. Using this methodology, it is possible to create distinct, visible boundaries between different grains in the microstructure as seen in Fig. 1.

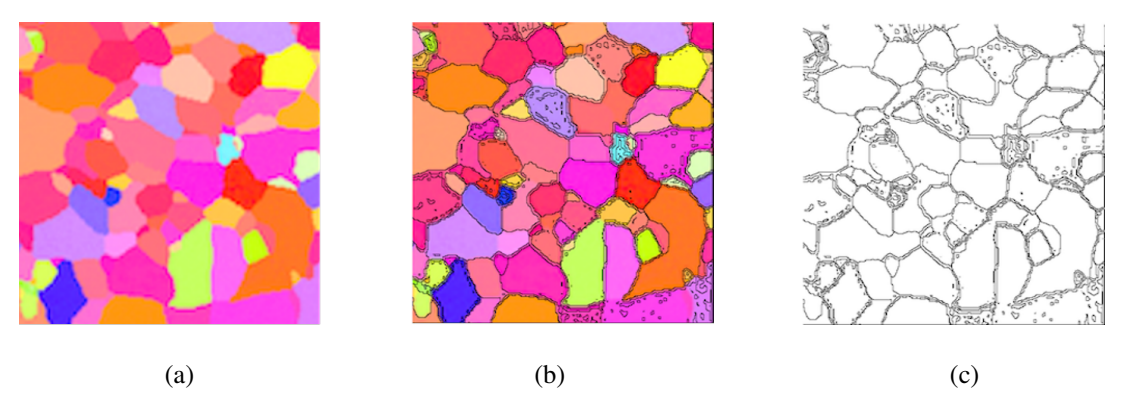


Fig. 1 Grain boundary identification of a Ti-7Al sample using tolerance-based neighbor analysis where (a) is before applying the filter, (b) is after the boundary filter is applied, and (c) is the network of the grain boundary

From this, it is possible to see that each of the grain is outlined in black, denoting the location of the grain boundary. It is necessary to address the black pixels that exist within the grain as they are considered to be noise that results from the conversion of EBSD data to a two-dimensional image. This is done by adjusting the tolerance value.

An alternative method to this similarity-based technique involves representing the RGB pixel intensity values in 3-D coordinate space. This makes it possible to calculate the Euclidean distance between neighboring pixels to establish whether they are of the same grain. A maximum distance is defined as 1 percent in order to identify when two neighboring pixels belong to different grains. Although this method presents some issues involving grain indexing compared to the previous method, this method has the potential to reduce the noise present in the tolerance-based method.

The benefit of outlining each grain is that the location and thickness of the boundary is preserved, meaning a volume fraction can be obtained for the boundaries themselves. This can be factored into the prediction of material properties by treating the boundaries as a distinct grain. The volume fraction of the grain boundaries can be determined by removing the grains from the image in order to leave only the identified boundaries, as seen in Fig. 1.

In the example of Fig. 1 when using the EBSD data for a Ti-7Al sample, it is found that the grain boundaries account for slightly more than twelve percent of the total area, a larger percentage than the most abundant grain for this sample, which only accounts for approximately eleven percent of the total area. With such a notable presence of the grain boundary, its effect on the material properties is likely significant to consider.

These techniques are compared to the existing Canny Edge Detector, an image processing tool in Python. The multi-stage process begins with a noise reduction filter which applies a Gaussian blur [12]. Applying a 5x5 Gaussian kernel blurs the image and hence reduces noise. Then, the intensity gradients between pixels are determined in both the vertical and horizontal directions to see how the intensity values are changing in terms of magnitude and direction. The magnitude (G) and the direction ( $\theta$ ) of the intensity gradient are determined using the following expressions [12].

$$G = \sqrt{G_x^2 + G_y^2}; \quad \theta = \arctan\left(\frac{G_y}{G_x}\right)$$
 (1)

where G is the magnitude of the intensity gradient with  $G_x$  and  $G_y$  being the x-component and y-component of the intensity gradients.  $\theta$  represents the direction of the intensity gradient [12]. At this stage, edges are identified but they vary in thicknesses. To address this, non-maximum suppression is applied to make the edge thicknesses more uniform. This is done by identifying the local maximum gradient values. These values indicate the location of the edge, and if the pixel does not have a local maximum gradient value, it is suppressed [12]. Lastly, hysteresis thresholding is applied. This step addresses the continuity of the edge lines. Two thresholds are determined, a minimum and maximum threshold. The maximum value denotes a sure-edge while the minimum value denotes a certain non-edge. The threshold values in this work are 125 and 50 because they yield the best visual separation of grains. These values were chosen because they have been found to consistently identify the expected grain boundaries. Once established, pixels that lie between these two threshold values are compared to neighboring pixels to determine whether they would be part of a continuous edge or instead part of a non-edge, meaning it is of the same grain as its neighbor [12]. The result of the Canny Edge Detection method can be seen in Fig. 2 below.

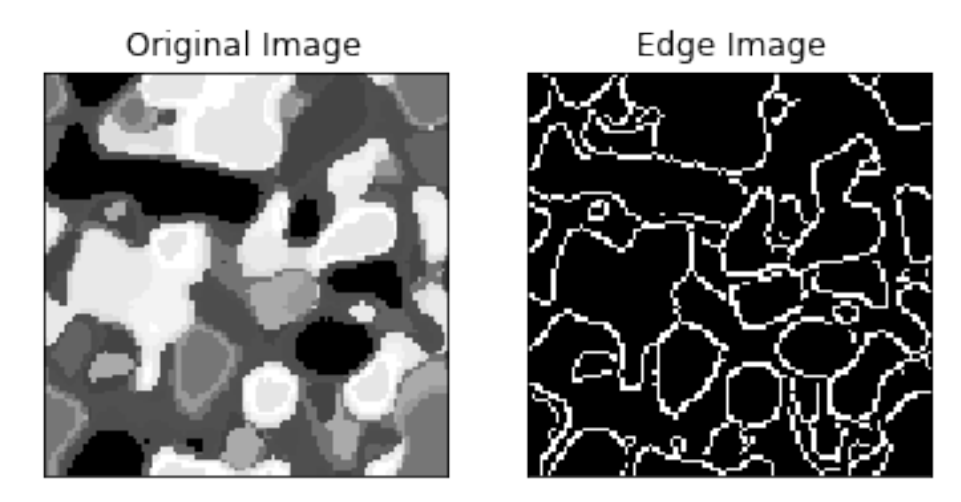


Fig. 2 Application of Canny Edge Detector on Ti-7Al sample with the Original (grayscale) and the Edge images

As can be seen, the information regarding grain orientation stored in the RGB color channels is lost when the original image is converted to gray scale. Additionally, this method requires experimentation with the threshold values in order to be as accurate as possible. If the maximum threshold value is too high, it is likely that not all edges will be identified. Conversely, if the minimum threshold value is too low, the grains will be grouped inaccurately. It will be necessary to compare the Canny Edge Detection technique with the proposed methodology described above to potentially refine this method. Once the grains are separated, it will be possible to compare grains of the same orientation but with different shapes using the shape moments invariants.

## III. Quantification of Microstructures using Shape Moment Invariants in 2-D and 3-D Space

This work quantifies grain shapes of microstructures using Hu moments. Hu defined seven sets of moments that are invariant to translation, rotation, and scale [13]. This work will initially consider all seven Hu moments in order to evaluate their corresponding sensitivity on the prediction of material properties. The mathematical definitions of these seven Hu moments are given as (2)-(8):

$$\phi_1 = \eta_{20} + \eta_{02} \tag{2}$$

$$\phi_2 = (\eta_{20} - \eta_{02})^2 + 4\eta_{11}^2 \tag{3}$$

$$\phi_3 = (\eta_{30} - 3\eta_{12})^2 + (3\eta_{21} - \eta_{03})^2 \tag{4}$$

$$\phi_4 = (\eta_{30} + \eta_{12})^2 + (\eta_{21} + \eta_{03})^2 \tag{5}$$

$$\phi_5 = (\eta_{30} - 3\eta_{12})(\eta_{30} + \eta_{12})[(\eta_{30} + \eta_{12})^2 - 3(\eta_{21} + \eta_{03})^2] + (3\eta_{21} - \eta_{03})(\eta_{21} + \eta_{03})[3(\eta_{30} + \eta_{12})^2 - (\eta_{21} + \eta_{03})^2]$$
(6)

$$\phi_6 = (\eta_{20} - \eta_{02})[(\eta_{30} + \eta_{12})^2 - (\eta_{21} + \eta_{03})^2] + 4\eta_{11}[(\eta_{30} + \eta_{12})(\eta_{21} + \eta_{03})]$$
(7)

$$\phi_7 = (3\eta_{21} - \eta_{03})(\eta_{30} + \eta_{12})[(\eta_{30} + \eta_{12})^2 - 3(\eta_{21} + \eta_{03})^2] - (\eta_{30} - 3\eta_{12})(\eta_{21} + \eta_{03})[3(\eta_{30} + \eta_{12})^2 - (\eta_{21} + \eta_{03})^2]$$
(8)

where  $\eta$  refers to the normalized central moments.

Assume that a single grain image is separated from a randomly oriented microstructure with a pixel area,  $A_g$ . The Orientation Distribution Function (ODF) values of the microstructure image, which are traditionally used to determine the material properties, can then be calculated through the pixels using the following expression:

$$ODF = \frac{VF}{q} \text{ where } VF = \frac{A_g}{A_t}$$
 (9)

VF represents the volume fraction where  $A_g$  is the image area of the grain, q is the volume normalization vector of the orientation space and  $A_t$  is the image area of the entire microstructure. For a randomly-oriented microstructure, the VF and consequently the ODF values will be the same for all grains. Given the large range of possible pixel intensity values, there is potential for noise in the EBSD sample images. Therefore, the grains that contain less than 15 pixels, a threshold used in a previous iteration of this work, will be filtered to reduce the noise present in the sample.

Before sensitivity analysis, all seven Hu moments are used when investigating the grain texture present in a microstructure sample. This work explores the different grain textures as well as the grid of grain boundaries in Titanium-Aluminum alloys, as seen in Fig. 3.

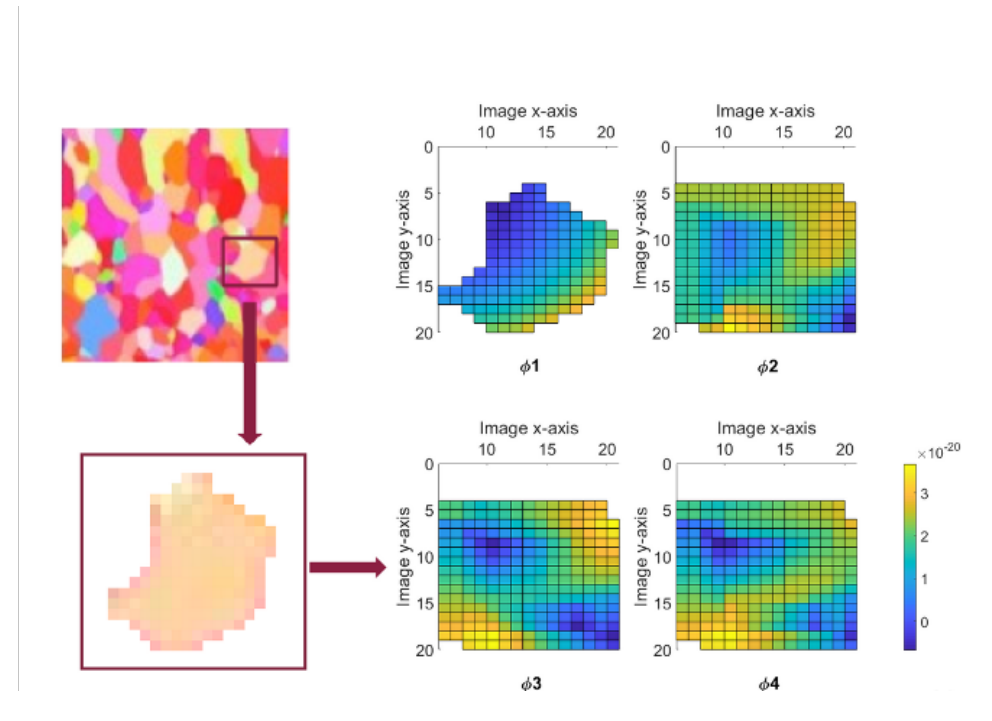


Fig. 3 Hu Moment calculation for selected grains of a forged Ti-7Al microstructure sample

Hu moments are calculated for each pixels of the image and it is plotted in Fig. 3. The final moment value is taken to be the summation of the Hu moment values for all the pixels. The surface plot of  $\phi_1$  in Fig. 3 explicitly displays the

expected shape of the grain as its formulation (Eq. 2) does not involve covariance prediction. Also, magnitude wise, it appears that the information carried by each additional Hu moment decreases. It arises the question whether it is possible for lower order Hu moments to be significant than higher order moments for uncertainty quantification. This will be investigated by the sensitivity analysis. Using the moment invariant representation, it will be possible to compare grains of the same orientation but with different shapes as well as to determine the shapes of the grain boundaries. The discoloration in Fig. 2 along the exterior of the individual grain indicates the grain boundary. Once identified, the grain boundaries can be grouped into a grain boundary network.

In order to calculate the material properties of the microstructure, it is traditionally necessary to know the volume fraction of each grain orientation. This can be performed using k-means clustering where pixels are grouped into a user-specified number of clusters based on the means of their intensities. To visualize this process, clusters of 15 major colors with each representing a unique orientation are separated from the original images, seen in Fig. 4. Once the number of unique grains is known, it is possible to obtain the volume fractions of each grain. Once the volume fractions are known, it is possible to obtain material properties using the ODF method. While the clustering method is effective for isolating individual grains, it does not include the consideration of the grain boundaries.

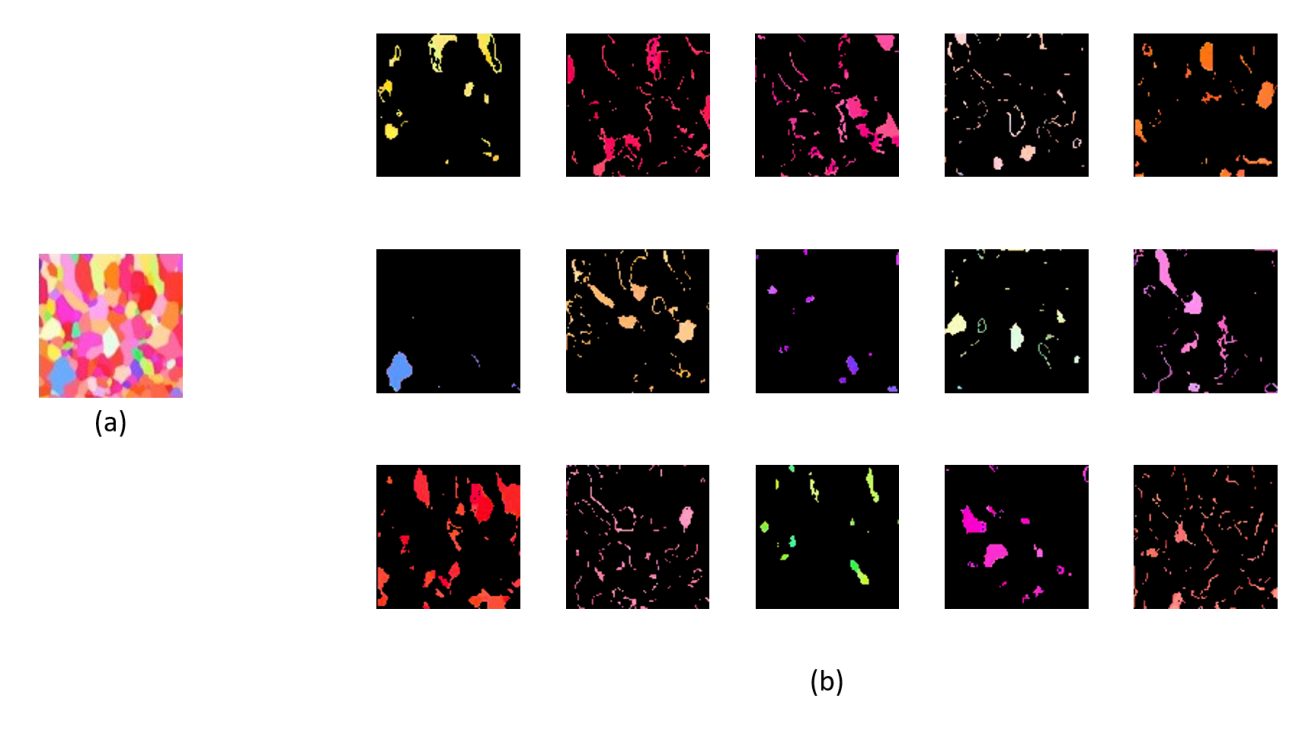


Fig. 4 (a) Original experimental image, (b) Separation of 15 clusters with each cluster indicating a unique microstructural orientation.

Although this method is useful for obtaining the volume fractions of different grain orientations, it is not possible to obtain the Hu moments of these clusters as they are comprised of multiple, distinct shapes. Here, the goal is to understand the effects of grains with the same orientation, but with different shapes. This work will separate singular grains from these clusters in order to obtain the Hu moments. Clustering will help this process by separating grains of the same orientation into their own image. Understanding the effects of grain shape and orientation through these methods will help predict and compare the material properties of different microstructures. Quantifying grain shapes in this manner proves to add difficulty when training a neural network because each microstructure sample has a different number of distinct grains. In order to obtain a more uniform set of neural network input values initially, it was decided to quantify the texture of the sample in addition to the grain boundary identification.

## IV. Results and Discussion

Two grain boundary identification methods were devised to examine the effect of incorporating the grain boundary into the prediction of the material properties of a given microstructure. The two methods differ in the level of detail to

which they separate the grain boundary grid. Both methods convert a sample microstructure image to a binary image of the grain boundary. These methods are shown in Fig. 5, where image (a) is the input image and (b) and (c) are the grain boundary grids obtained using the neighbor analysis and Euclidean distance methods, respectively. The grains in these grids are converted to black pixels to show the grain boundary in white. Previously, the grain boundaries were shown in black with the actual grains in white, but the grain boundaries required nonzero pixel intensity value in order to offer the necessary input to obtain the Hu moments.

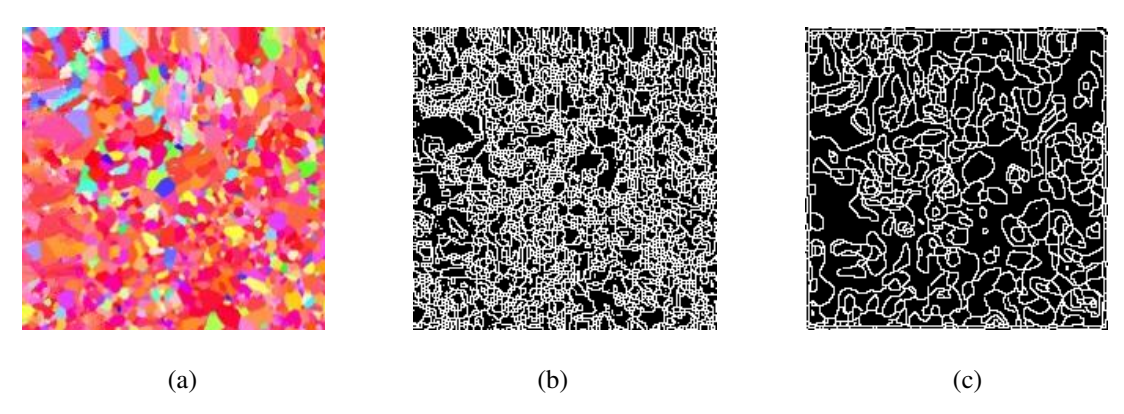


Fig. 5 Grain boundary filtration where (a) is before applying the filters, (b) is the the grain boundary grid using the Neighbor Analysis method (c) is grain boundary grid using the Euclidean Distance method

As can be seen from the two grain boundary grids, the neighbor analysis method is more strict in terms of determining the difference between adjacent grains. This is likely because this method examines each color channel separately to determine whether neighboring pixels belong to the same grain. Meanwhile, the Euclidean distance method looks at the intensity magnitude of the three color channels combined. Since the pixel intensity values are normalized, the Euclidean distance value requires a rather small tolerance value in order to distinguish between adjacent grains.

Once these two methods were defined, neural networks were trained using sample image data to determine whether the inclusion of the grain boundary identification methods improved the ability to predict the homogenized material properties of the microstructure. Due to the computational expense of obtaining additional reconstructed image data, a data set consisting of 100 Ti-7Al EBSD images were used. Bayesian Regularization was selected to train the neural network for this work because it can perform good generalization for small data sets [15]. The input for the neural networks were the Hu moments obtained for the overall image, rather than the Hu moments of each grain. As mentioned above, the Hu moments quantify the image based on the pixel intensity values in the three color channels, making it possible to quantify the microstructural features of a sample image with the seven Hu moments. The Hu moments can also be obtained for the black and white grain boundary grids. Hu moments were used as input data to predict the material properties, specifically the Young's modulus and yield strength values,  $E_{11}$ ,  $E_{22}$ , and  $\sigma_{\nu}$  of the sample.

In order to determine the effectiveness of the two grain boundary neural networks, an initial Bayesian Regularization neural network was trained, using only the Hu moments of the unchanged, color image. Once finished, the same process was repeated for the two grain boundary identification methods using both the Hu moments of the color image and those of the grain boundary grid image. The neural network was trained using the 100 image samples as well as their corresponding experimental material properties,  $E_{11}$ ,  $E_{22}$ , and  $\sigma_y$ . These samples were split into a 70 % training set, a 15% validation set, and a 15% test set. There were 8 hidden layers used to generate all three artificial neural network functions.

The initially trained neural networks underwent a sensitivity analysis to determine the impact of Hu moments. The result of the sensitivity analysis, as seen in Fig. 6, showed that only the first Hu moment had a significant impact on the prediction of the material properties. This supports a previously reported data where the first Hu moment was found to be more significant than the others in magnitude [16]

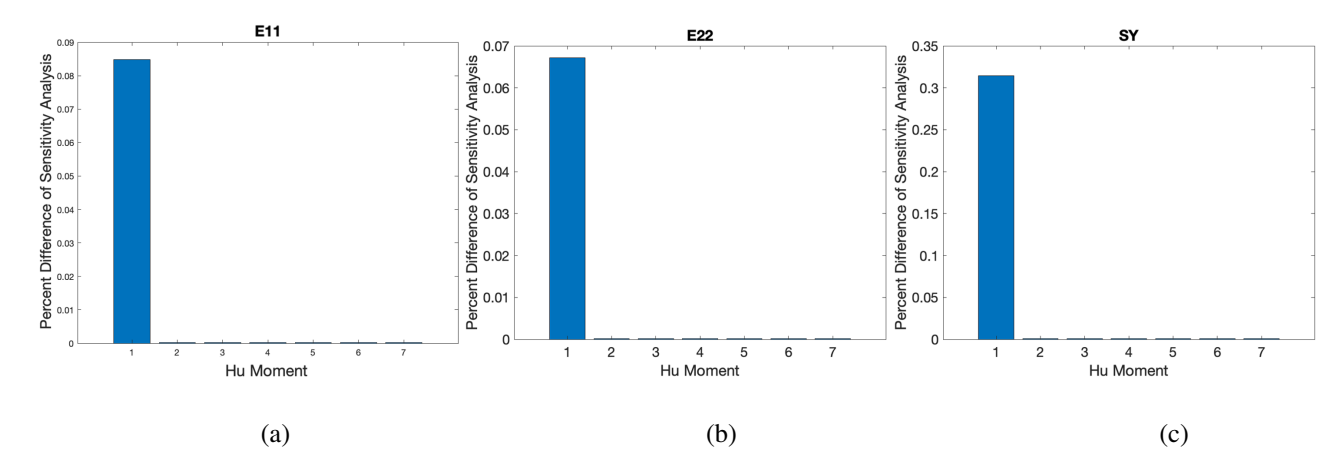


Fig. 6 Sensitivity analysis of different moment invariant input on material property outputs where (a) is sensitivity on  $E_{11}$  (b) is sensitivity on  $E_{22}$  (c) is sensitivity on  $\sigma_v$ 

For  $E_{11}$ , changing the first Hu moment by 5 percent changed the predicted value by slightly less than 0.09 percent. Similarly for  $E_{22}$  and  $\sigma_y$ , the same input change yielded a change in the prediction by roughly 0.07 and 0.3 percent, respectively. While these values are low, they become significant when compared to the sensitivity results of the other six Hu moments. This is likely due to the large decrease in magnitude of each Hu moment after the first one. This can be seen visually in Fig. 3, where the plot of the first Hu moment most directly reflects the input grain. It is also important to note that  $\sigma_y$  experiences the largest effect of the sensitivity analysis. An explanation could be that the Young's modulus value is a metric of the linear elastic region, and the yield strength resides in the elasto-plastic region.

The neural networks were retrained in order to reduce the input variables based on the results of the sensitivity analysis. Three artificial neural network functions were created to evaluate the predictive potential of the grain boundary identification methods compared to the method that excludes identification of the grain boundaries. The first function included only the first Hu moment of the overall microstructure. The following two functions used the first Hu moment of the overall microstructure and the Hu moment of either the neighbor analysis or Euclidean distance grain boundary. Fig. 7 shows the regression plots of each of the three neural networks.

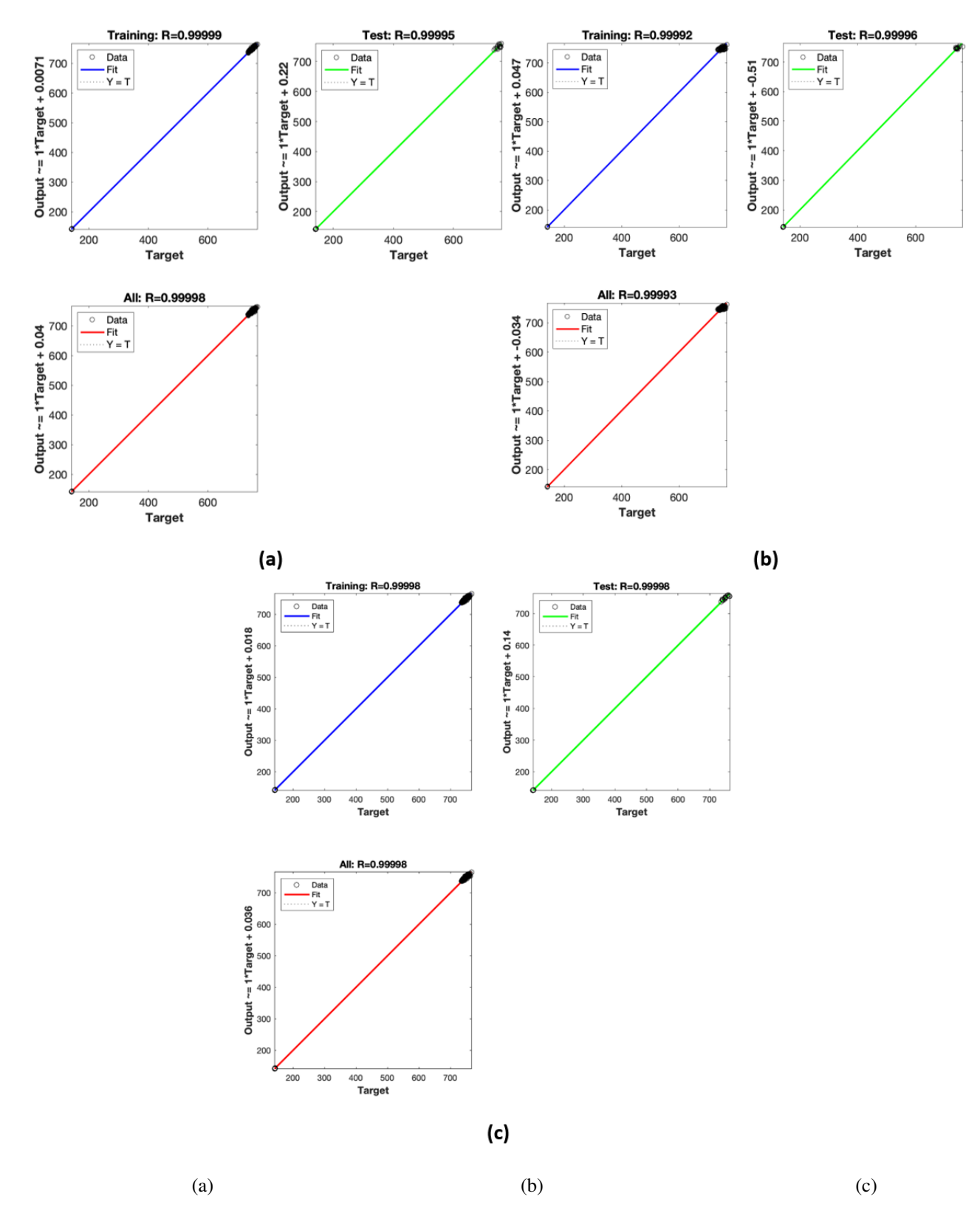


Fig. 7 Regression plots of the training, test, and overall data sets where (a) the no grain boundary method, (b) neighbor analysis method, and (c) the Euclidean distance method

As can be seen in Fig. 7, the fitting performance of each neural network is satisfactory. It is possible, through comparison of the regression plots, that the fit of the two grain boundary identification methods are slightly better than that of the control method. However, it was necessary to compare the output of each of these methods to the experimental results to determine the performance of each neural network function. The average percent difference between the experimental data and the respective output of each neural network function can be seen in Fig. 8.

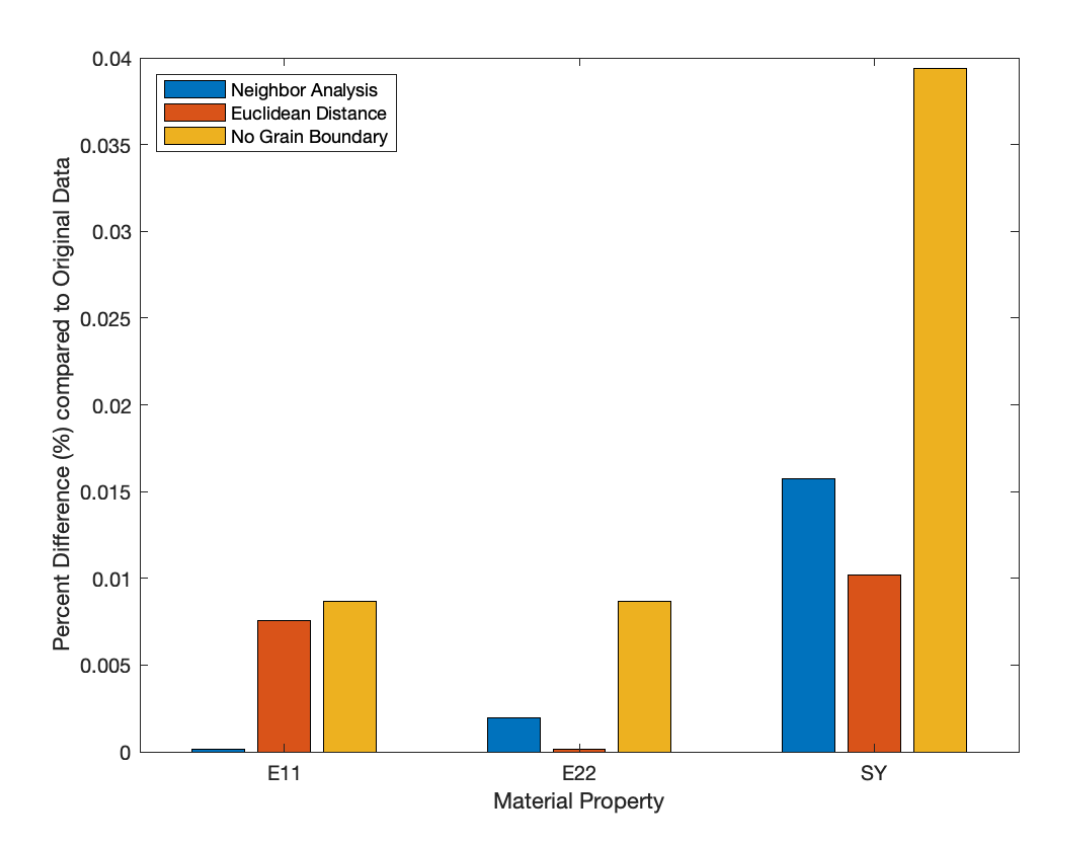


Fig. 8 Percent difference compared to the experimental data of the material properties for the neighbor analysis method (Blue), the Euclidean distance method (Orange), and the no grain boundary method (Yellow)

When comparing the material property outputs of the three different neural network functions to the experimental data, the function that does not consider the effect of the grain boundary has a higher percent difference than the two functions that do. While this difference is below 0.01 % for both Young's modulus values, the percent difference for  $\sigma_{\rm v}$  is significantly higher for the case that does not include the grain boundary consideration. In the two cases where the grain boundary is considered, the neural network outputs are very similar to the experimental material properties, particularly for the Young's modulus values. It is important to note that the percent difference for the neighbor analysis function is below 0.005 % for both  $E_{11}$  and  $E_{22}$ . Additionally, both the neighbor analysis and Euclidean distance functions produce differences of less than 0.02 \%. Previously, the percentage difference was found to be around 5\% for the same material properties between experimental and computational images using crystal plasticity simulations [17]. The reason why this difference was higher can be attributed to the model uncertainty of crystal plasticity simulations. When training a neural network, it is shown that considering the grain boundary of a microstructure leads to a function that outperforms the case where the grain boundary grid is not used as an input variable. In terms of determining whether one grain boundary identification method is better than the other, it is currently unclear based on the results of this analysis. The neighbor analysis, on average, outperforms the Euclidean distance method when predicting the two Young's modulus values. However, the Euclidean distance method outperforms that of the neighbor analysis for the prediction of the yield strength. In order to further evaluate the effectiveness of these neural network functions, the propagation of microstructure uncertainty arising from processing conditions was examined as well.

To represent the microstructure uncertainty, three normally distributed data sets, consisting of 1000 samples, were generated from the average of the experimental Hu moments with a maximum perturbation of 5 %. The first set corresponded to the texture of the microstructure in the three color channels. The second two sets corresponded to the Hu moments obtained from the grain boundary grids of the neighbor analysis and Euclidean distance methods, respectively. The histograms of these input data sets can be seen in Fig. 9. It is worth noting that the magnitude of the Hu moments in each of these data sets reflect the pixel intensity values of the images, explaining how the first Hu moment of the three color channel image is higher than those of both grain boundary grid images. Additionally, it is possible to see that the overall Hu moment values of the neighbor analysis grain boundary are higher in magnitude than those of the Euclidean distance grain boundary, relating to the overall presence of white pixels in Fig. 5 (b) and (c), respectively.

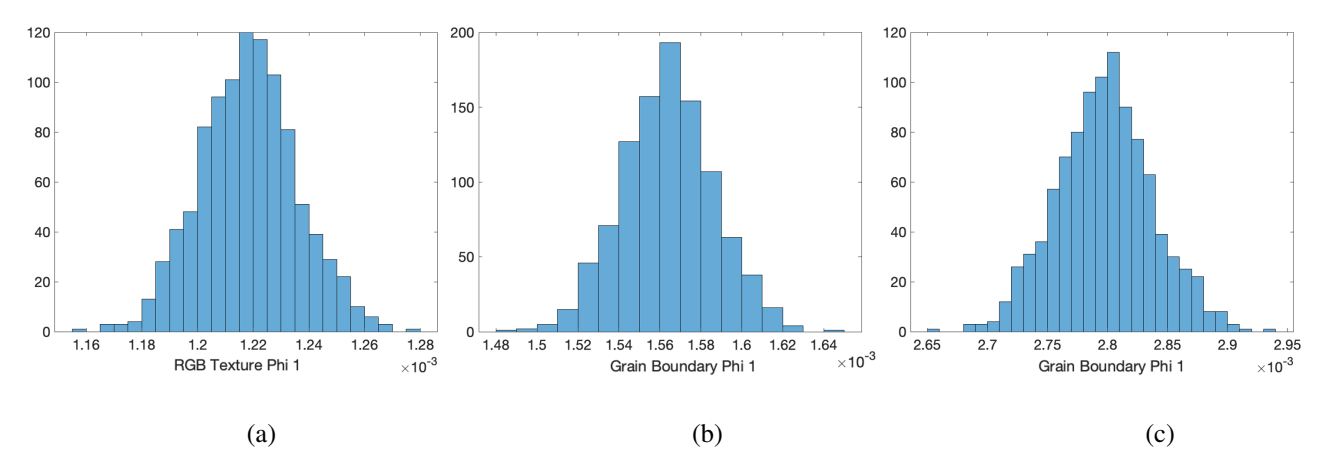


Fig. 9 Histogram of shape moment invariant inputs to the three different neural networks where (a) is the first RGB Hu moment of the overall image, (b) shows the microstructural features of the neighbor analysis grain boundary grid, and (c) shows the microstructural features of the Euclidean distance grain boundary grid

These normally distributed data sets were then used as input to the three neural network functions to generate a set of 1000 material property outputs for each function. The distribution of the  $E_{11}$  values predicted by each neural network function can be seen in Fig. 10.

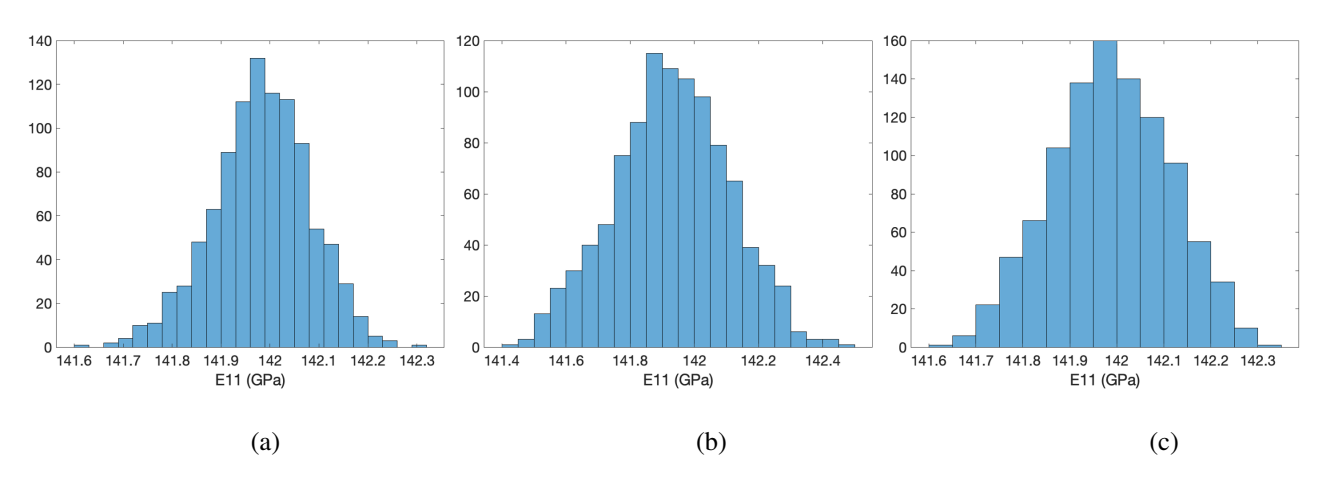


Fig. 10 Histogram of  $E_{11}$  for 1000 normally distributed sample inputs obtained using (a) the no grain boundary, (b) the neighbor analysis, and (c) Euclidean distance methods

The spread of the outputs have a difference of 0.7 GPa for the no grain boundary method, 1.0 GPa for that of the neighbor analysis method, and 0.8 GPa for the Euclidean distance method. The results are similar for the  $E_{22}$  output of each function, as can be seen in Fig. 11. It is also necessary to note that the outputs for both Young's modulus values

agree well with normal distribution for all the neural network functions, suggesting a quasi-linear relationship between the Hu moment input and the two Young's modulus output.

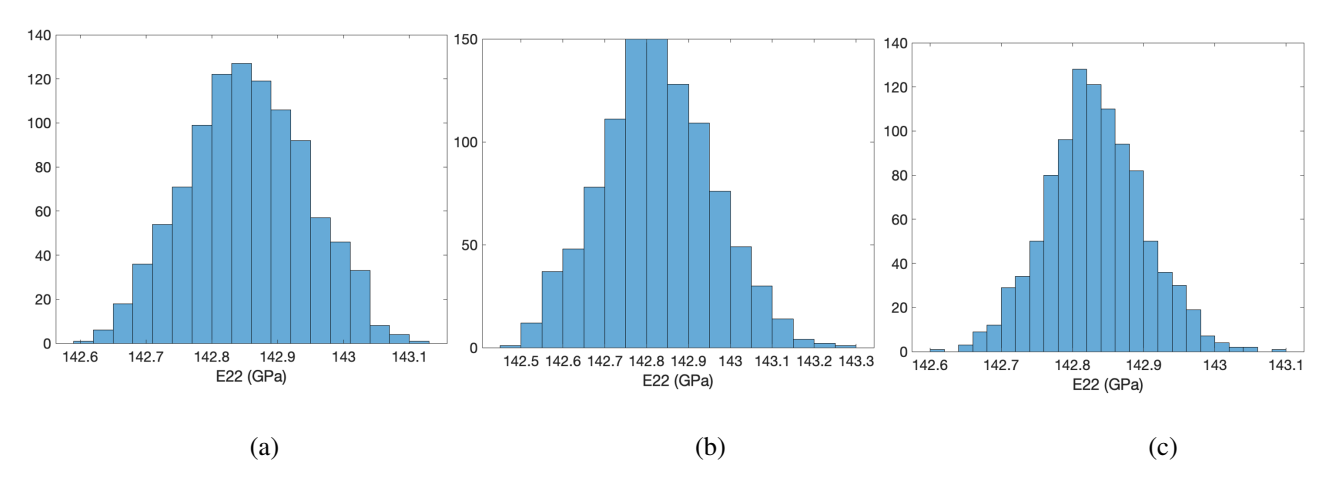


Fig. 11 Histogram of  $E_{22}$  for 1000 normally distributed sample inputs obtained using (a) the no grain boundary, (b) the neighbor analysis, and (c) Euclidean distance methods

However, when examining the histogram results of the yield strength, the outputs of the neural network functions are no longer normally distributed, as seen in Fig. 12. The output curve is shifted left to lower side of the range of values. It is also possible to see that the spread of possible outputs is much larger than those of the two Young's modulus values with ranges of 9 MPa, 16 MPa, and 8 MPa for the no grain boundary, neighbor analysis, and Euclidean distance histograms, respectively. The distribution of values in the histogram suggests that the relationship for the yield strength and the Hu moments is more complex than for the two Young's modulus values.

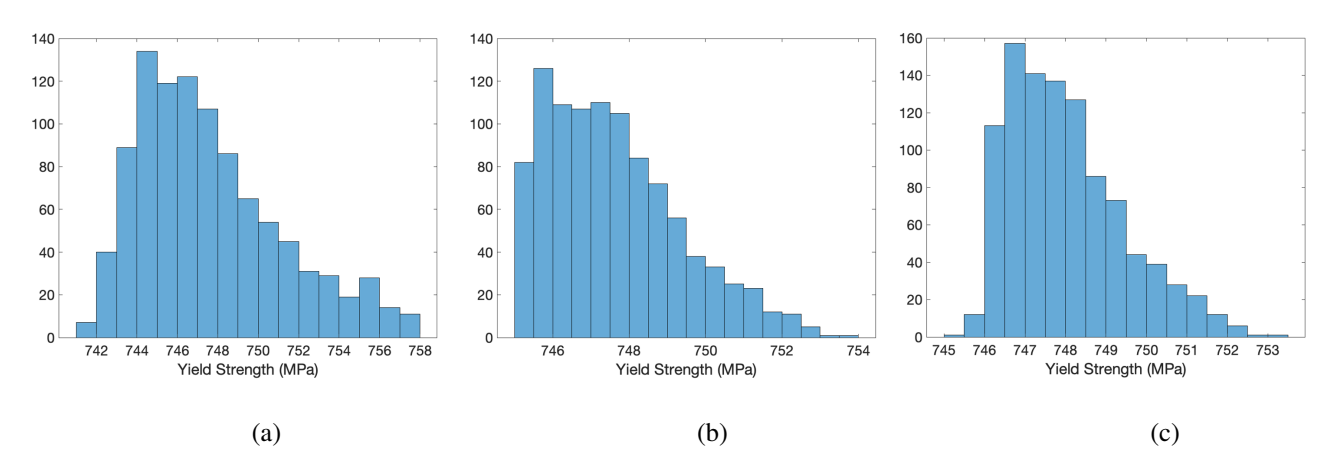


Fig. 12 Histogram of yield strength for 1000 normally distributed sample inputs obtained using (a) the no grain boundary, (b) the neighbor analysis, and (c) Euclidean distance methods

The method of quantifying a two-dimensional Ti-7Al microstructure using shape moment invariants can then be expanded to quantify a three-dimensional microstructure sample examining the cross-sections of the sample. It would also be possible to apply the grain boundary identifying methods, but it would be necessary to apply this method for all three planes in order to prove the continuity of the grain boundary in a reliable way. Once a three-dimensional sample is quantified using this method, similar neural networks could be trained using these shape moment invariants to predict the material properties of the sample.

#### V. Conclusion

The present work addresses data processing techniques involving k-means clustering, grain boundary detection, and shape moment invariants. This work explores two different methods of identifying the grain boundaries in EBSD data images of metallic microstructures. The first is developed based on pixel neighbor analysis using the pixel intensity values in each of the RGB color channels. This method preserves the grain orientation information, making it possible to separate unique grain orientations while still identifying the boundaries between different grains. While this method is promising, it needs additional refinement that addresses the uncertainty created during image processing. Effects of grain shape for different orientations are investigated through the utilization of shape moment invariants. This methodology is based on the application of a physical concept that quantifies the shape of individual grains. Once unique grain orientations are isolated using the clustering technique, it is possible to isolate individual grains to obtain their Hu moments. Different shapes affect the homogenized material properties as well as the material's response to crack propagation and other important phenomena.

Future work will expand the two-dimensional analysis to predict material properties on 3D microstructures with consideration for grain boundaries, shapes, and orientations in three-dimensional space. Additionally, work will be done to implement a machine learning technique to reverse the process of quantifying a microstructure sample. The goal will be to quantify the grain boundary network, seen in Fig. 1(c), and use it to create synthetic microstructures with a parametric representation by inputting Hu moment values. This process will help in refining the design of microstructures and could potentially provide insight to the effects of different processing parameters in the manufacturing stage.

## VI. Acknowledgments

RC, AS, and PA would like to acknowledge the financial support from the National Science Foundation (NSF) CMMI Grant # 2053840. The support from the Commonwealth of Virginia Innovation Project E-059 is also acknowledged. Finally, the authors would also like to thank Professor John Allison (Department of Materials Science and Engineering, University of Michigan) for providing the experimental images.

#### References

- [1] Wright, S. I. and Nowell, M. M., "EBSD image quality mapping," *Microscopy and microanalysis*, Vol. 12, No. 1, 2006, pp: 72-84.
- [2] Wright, S. I, "Fundamentals of automated EBSD", *Electron backscatter diffraction in materials science*, 1st ed., Vol. 2, Springer, Boston, MA, 2000, pp. 51-64.
- [3] Schwartz, A.J., Kumar, M., Adams, B.L. and Field, D.P. eds., *Electron backscatter diffraction in materials science*, Vol. 2, Springer, New York, 2009, p. 403.
- [4] Adams, B. L., S. I. Wright, and Karsten Kunze, "Orientation imaging: the emergence of a new microscopy," *Metallurgical Transactions A*, Vol. 24, No. 4, 1993, pp: 819-831.
- [5] Dingley, D. J., and V. Randle, "Microtexture determination by electron back-scatter diffraction," *Journal of materials science*, Vol. 27, No. 17, 1992, pp. 4545-4566.
- [6] Humphreys, F. J., "Characterisation of fine-scale microstructures by electron backscatter diffraction (EBSD)," Scripta materialia, Vol. 51, No. 8, 2004, pp. 771-776.
- [7] Carpenter, D. T., J. M. Rickman, and K. Barmak. "A methodology for automated quantitative microstructural analysis of transmission electron micrographs." *Journal of applied physics*, Vol. 84, No. 11, 1998, pp. 5843-5854.
- [8] Mahadevana, S. and D. Casasent "Automated image processing for grain boundary analysis" *Ultramicroscopy*, Vol. 96, Iss. 2, pp: 153-162, August, 2003.
- [9] Ramsahoye, B. H. "Nearest-neighbor analysis." DNA Methylation Protocols. Springer, Totowa, NJ, 2002. pp: 9-16.
- [10] Pinder, D., I. Shimada, and D. Gregory. "The nearest-neighbor statistic: archaeological application and new developments." American Antiquity, Vol. 44, No. 3, 1979. pp: 430-445
- [11] Choudhury, K. Roy, P. A. Meere, and Kieran F. Mulchrone. "Automated grain boundary detection by CASRG." *Journal of Structural Geology* Vol. 28, No. 3, 2006. pp. 363-375.
- [12] Sahir, S., "Canny Edge Detection Step by Step in Python Computer Vision," toward data science, January 25, 2019.
- [13] Hu, M., "Visual pattern recognition by moment invariants," *IRE transactions on information theory*, Vol. 8, No. 2, pp: 179-187, 1962.
- [14] MacSleyne, J. P. "Moment invariants for 2-D and 3-D characterization of the morphology of gamme-prime precipitates in nickel-base superalloys," Ph.D. Dissertation, Carnegie Mellon University, Pittsburgh, PA, 2008.
- [15] Foresee, D.F., and M. T. Hagan. "Gauss-Newton approximation to Bayesian learning." *Proceedings of the International Joint Conference on Neural Networks*, June, 1997.
- [16] Senthilnathan, A., and P. Acar, and Marc De Graef. "Markov Random Field based microstructure reconstruction using the principal image moments." *Materials Characterization* Vol. 178, 2021: 111281.
- [17] Senthilnathan, A., and P. Acar. "Shape Moment Invariants as a New Methodology for Uncertainty Quantification in Microstructures." AIAA Scitech 2021 Forum. 2021.
- [18] MacSleyne, J. P., J. P. Simmons, and M. DeGraef, "On the use of 2-D moment invariants for the automated classification of particle shapes," *Acta Materialia*, Vol. 56, No. 3, 2008, pp. 427-437.
- [19] Sundararaghavan, V., and N. Zabaras, Classification and reconstruction of three-dimensional microstructures using support vector machines, *Computational Materials Science*, Vol. 32, No. 2, 2005, pp. 223-239.
- [20] Acar, P., and V. Sundararaghavan, A Markov random field approach for modeling spatio-temporal evolution of microstructures, Modelling and Simulation in Materials Science and Engineering, Vol. 24, No. 7, 2016, 075005.